Catena 207 (2021) 105705

Contents lists available at ScienceDirect

Catena

journal homepage: www.elsevier.com/locate/catena

^{226}Ra, ^{228}Ra and ^{40}K as tracers of erosion and accumulation processes: A 3-year study on a beach with different sediment dynamics

A.C. Arriola-Velásquez [a], A. Tejera [a,*], J.G. Guerra [a], W. Geibert [b], I. Stimac [b], F. Cámara [c], H. Alonso [a], J.G. Rubiano [a], P. Martel [a]

[a] Department of Physics, Instituto Universitario de Investigación en Estudios Ambientales y Recursos Naturales i-UNAT, Universidad de Las Palmas de Gran Canaria, Campus de Tafira, 35017 Las Palmas de Gran Canaria, Spain
[b] Alfred Wegener Institute, Helmholtz Centre for Polar and Marine Research, Bremerhaven, Germany
[c] Dipartimento di Scienze della Terra, Università degli Studi di Milano, via Sandro Botticelli 23, 20133 Milano, Italy

ARTICLE INFO

Keywords:
Radionuclides
Tracers
Coastal sediments
Beach
Erosion/accumulation

ABSTRACT

The aim of this study is to analyse the role of natural radionuclides ^{226}Ra, ^{228}Ra, ^{40}K and unsupported ^{210}Pb (^{210}Pb$_{ex}$), as erosion and accumulation process tracers. For this purpose, a complex system, including both the characteristic dynamics of a closed beach and those associated with a beach open to wave action, was studied. A 3-year study of monthly variation of ^{226}Ra, ^{228}Ra, ^{40}K and ^{210}Pb$_{ex}$ was carried out at Las Canteras beach, on the Island of Gran Canaria (Spain), covering several erosion and accumulation periods. A correlation analysis, ANOVA test and Tukey's Honestly Significant Difference (HSD) Test proved that the marine erosion and accumulation agents influenced the activity concentration values found for the different radionuclides. Moreover, the geochemical analysis of samples from maximum and minimum activity concentration values showed that the natural radionuclides studied could be suitable tracers for studying beach sediment dynamics in erosion and accumulation periods.

1. Introduction

Natural radioactivity on the Earth's surface has different origins; principally it is generated by the primordial elements in the Earth's crust. The rest is generated by the interaction of cosmogenic radiation with the atmosphere and its deposition onto the planet surface by different processes. The most common radionuclides on the Earth's crust are ^{40}K and those that come from the radioactive decay chains of ^{238}U and ^{232}Th. The geochemical composition of the Earth's crust influences the different types of sediments and rocks that crop out at the surface around the world, varying its radioactivity levels from one place to another. In coastal areas, the geochemical and geophysical conditions also influence in the levels of radioactivity that can be found in its sediments. For example, in areas where permeable sediments can be found, processes such as tidal pump affect the coastal aquifers and create a flow of water known as submarine groundwater discharges (SGD) (Burnett et al., 2003; Moore, 2007). In these cases, when salty water gets in contact with the surface sediments of the aquifer Ra isotopes are transferred to the water from the sediments. Therefore, these sediments will present a lower activity concentration or Ra radionuclides than they normally would. Within this framework, some studies have been focused on the use of natural radionuclides in coastal waters as tracers of possible sediment derived inputs of nutrients or contaminants in the ocean (Kipp et al., 2020; Sanial et al., 2015; Tamborski et al., 2018). Other studies have focus on the measurement of natural radionuclides contained in sediments to assess the sediment transfer time in river systems as well as river flood reconstructions (Chabaux et al., 2012, 2006; Yang et al., 2013). Moreover, there are studies that focused on the use of natural radionuclides in sediments as tracers of sediment sources and transport pathways in coastal areas (Bezuidenhout, 2020; Huang et al., 2013; Lin et al., 2020; Thereska, 2009; Wang et al., 2018). In addition, some studies have also used the natural radionuclides content in core sediments to measure sedimentation rates, sediment redistribution or sediment dating (Giffin and Corbett, 2003; Li et al., 2021; Sun et al., 2020). All of these studies are examples that show the relevance of using natural radionuclides as tracers of sediment dynamics and processes related to it.

In the case of Las Canteras beach, located in El Confital Bay in the

* Corresponding author.
E-mail address: alicia.tejera@ulpgc.es (A. Tejera).

https://doi.org/10.1016/j.catena.2021.105705
Received 31 May 2021; Received in revised form 26 August 2021; Accepted 29 August 2021

north of the Island of Gran Canaria (Spain), previous studies have established a baseline of environmental radioactivity in sand samples and algae arrivals (Arnedo et al., 2013; Arriola-Velásquez et al., 2019; Tejera et al., 2019). Las Canteras beach is divided into three arches and has a rocky bar offshore that protects the northern and central arches (Fig. 1). This bar is not a whole block and presents openings that create different sections, predominantly in the central arch. Therefore, the part of the beach that is most protected against wave action by the natural offshore rocky bar is the northern arch, whereas the southern arch is totally exposed to the wave action (Alonso, 1994, 1993; Alonso and Vilas, 1996). In this framework, the 1 year study by Arriola-Velásquez et al. (2019) provided information about the spatial distribution of natural radionuclides ^{226}Ra, ^{232}Th and ^{40}K, along the beach. The sampling points with lower activity concentrations of these radionuclides were in the parts of the beach with no protection from the bar, while the sampling points that were fully protected by the rocky bar presented higher activity concentration values. The sampling points that were in front of the openings of the bar displayed intermediate activity concentration values. This seemed to indicate that the spatial distribution of these natural radionuclides was related to the different sediment dynamics that can be found on Las Canteras beach, depending on the presence or absence of the natural offshore rocky bar and its openings. Moreover, in that work, a temporal variability study was performed for the first time. The ^{226}Ra/^{228}Ra ratio proposed by Dai et al. (2011) was used for that purpose. According to their study, ^{228}Ra and ^{226}Ra are more present in the crystal framework of clay minerals, but the carbonate and exchangeable phases contain more ^{228}Ra. Thus, accretion or erosion periods could be measured by a change in the ratio between ^{226}Ra and ^{228}Ra, assuming the natural ratio ^{232}Th/^{238}U. Therefore, during accumulation periods the input of ^{228}Ra would be higher and the ratio would have a value below 1. During erosion periods, on the contrary, the ratio would have a value above 1. In the case of Las Canteras beach some crystals from clay minerals and zeolites had been found in the north part of it (Mangas and Julià-Miralles, 2015). Hence, the use of this ratio as a tracer of erosion and accumulation period seemed suitable for the study of Arriola-Velásquez et al. (2019). The results showed a constant accumulation period when a full protection of the bar was present. However, for the open part of the beach and the parts located in front of the opening, the results exhibited the need for a further temporal analysis to better understand the temporal variability of radionuclides in these parts of the beach.

The results obtained for the spatial and temporal variability of the natural radionuclides at Las Canteras beach in 2019 seemed to indicate that the radionuclides studied were tracing the sediment dynamics that had been studied for this region. According to these previous studies, the beach presents seasonal variability in its sedimentary budget (Alonso, 1994, 1993; Alonso and Vilas, 1996). In erosion periods, the southern arch, being totally exposed to the wave action, loses a large amount of sediments that suffer a lengthwise transport to the northern and central arch. On the other hand, in accumulation periods, the whole beach receives an inflow of sediments. Under these circumstances, some berms appear in the northern arch and a lengthwise transport can occur to the southern arch. The sediments that arrive on the beach come from the geological environment, basic volcanic rocks from La Isleta, in the northeast of El Confital bay, phonolitic lava flow from the southwestern side of the bay, basic rocks and magnetite from the mouth of La Ballena ravine in the south part of the beach, submerged sandbars located between the bathymetric curve of 50 m and the beachfront and the natural offshore calcarenite rocky bar (Balcells et al., 1990; Schmincke, 1993). Some calcimetry and petrological analyses of the beach sand, as well as the geological composition of El Confital Bay define the different geological materials that can be found along Las Canteras beach. The northern arch presents a higher bioclast and calcareous content than the southern arch. Nevertheless, the northern part of the beach has a higher content of calcarenite that contains mainly feldspar crystals in its terrigenous part. Therefore, feldspars are also accumulated in the northern part of the beach. On the other hand, the outlet of the ravine that ends in Las Canteras beach is located in the southern part. Hence, this part tends to accumulate clinopyroxenes and other heavy minerals, such as olivine, amphiboles and Fe-Ti oxides that come from this ravine while the lighter lithics are redistributed along the beach (Alonso, 1993; Alonso and Pérez Torrado, 1992; Mangas and Julià-Miralles, 2015; Medina et al., 2006). All of these differences between one part of Las Canteras beach and another make it an ideal natural laboratory to monitor the changes in natural radionuclides associated with distinct sediment dynamics. The beach presents two parts with different sediment dynamic and composition. The south part is opened to the wave action and tends to accumulate heavy minerals. The northern part is

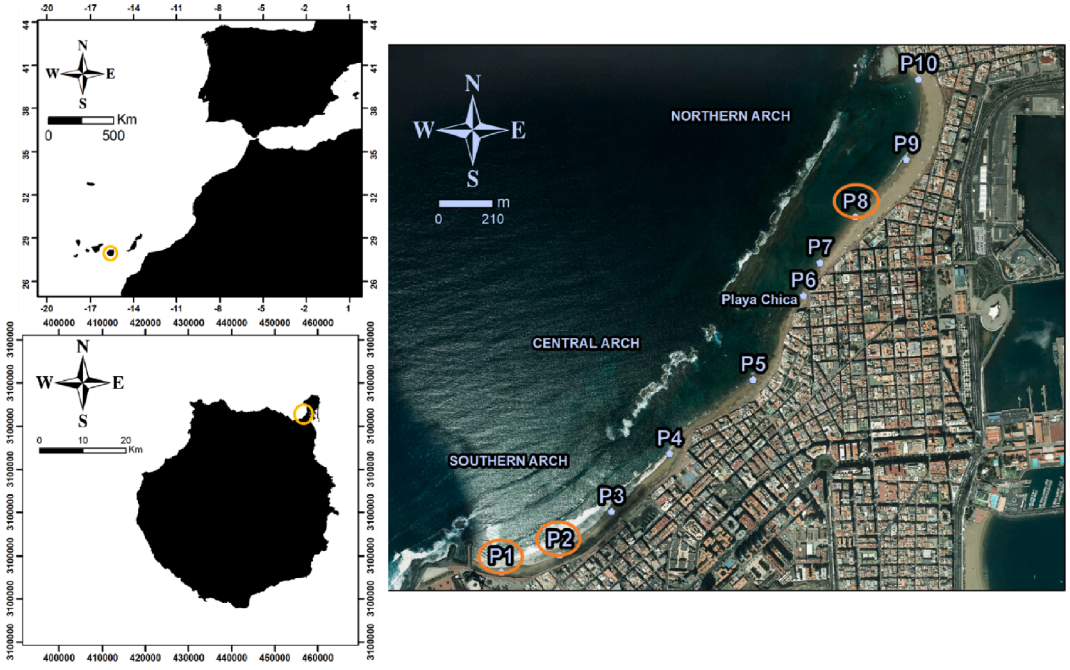

Fig 1. Location of the study region and the sampling points in Las Canteras beach. Coordinates are in the UTM system.

protected against the wave action by the natural offshore rocky bar and presents more calcarenite and organic material. Therefore, the results obtained in this beach could resemble to the evaluation of radiotracers of sediment dynamics in two different beaches with different marine dynamics and mineralogical composition. Hence, radiotracers that trace sediment dynamics in both parts of the beach would have a wider use and could be suggested as tracers that can be used in other parts of the world. In addition, radiotracers that only seemed to work in one part of the beach could be suggested as tracers of sediment dynamics of beaches with similar characteristics to one the different parts of Las Canteras beach.

In essence, previous studies at Las Canteras beach have provided information on the spatial variability of environmental radionuclides which seems to follow the dynamics under which the different parts of the beach are subjected. However, a further temporal analysis is necessary, to prove the viability of natural radionuclides as tracers of beach sediment dynamics. Therefore, the aim of this work is to provide a deeper analysis of the temporal variability of natural radionuclides at Las Canteras beach. For this purpose, the changes in activity concentrations of natural radionuclides will be analysed over a period of 3 years. Moreover, the relations between these variations in activity concentration and different erosion and accumulation agents, such as significant wave height or wind speed, will be evaluated. Finally, the geochemical differences in samples from erosion and accumulation periods will be studied. Las Canteras beach was selected for this study due to the combination of the characteristic dynamics of a closed beach and those associated with a beach open to wave action. This would allow the results of this work to be applied to other places around the world.

2. Material and methods

2.1. Sample collection and preparation

A total of 360 samples were taken during the study period. Sand collection was undertaken monthly for three years, from September 2016 to August 2019. Ten samples were selected for each campaign (Fig. 1): four in the southern arch, one in the central arch, one in Playa Chica and the last four in the northern arch.

In order to study the marine interactions with the distribution of radionuclides, superficial samples were taken during low tide in the intertidal zone of Las Canteras beach. At each sampling point, a square of 1 m^2 was drawn and, after mixing in situ, samples were taken from the superficial sand (between 0 and 5 cm depth). After the samples were taken to the laboratory, they were dried at 80 °C for 24 h. They were then sieved through a 1 mm mesh size to homogenise them and kept inside PVC-trunk conical containers, filled to 40 cm^3. They were sealed with aluminium strips, because they are impermeable to radon gas. Finally, the samples were stored for a duration of approximately one month before measurement to allow secular equilibrium between ^{226}Ra and ^{222}Rn and its short-lived progenies (as ^{214}Pb is used for determining ^{226}Ra) (Bezuidenhout, 2013).

2.2. Meteorological, oceanographic and PM_{10} data

To establish if variations in environmental conditions during the different campaigns affected the variations in activity concentration of radionuclides, the effect of environmental conditions were studied. For this, hourly atmospheric conditions (atmospheric pressure, air temperature, relative humidity and PM_{10} levels) were taken from a station belonging to the network of surveillance and control of air quality, run by the Canary Islands Government, during campaign hours. In addition, data of wave approach direction and significant wave height at low tide in the distinct campaigns were taken from a buoy of the Puertos del Estado surveillance network, belonging to the government of Spain. Wind approach direction and wind speed data were also obtained from the same station at Puertos del Estado.

2.3. Gamma emission analysis

The determination of radionuclides in sand samples by gamma spectrometry analysis was carried out using a Canberra Extended Range (XtRa) Germanium spectrometer (model GX3518), with 38% relative efficiency with respect to a 3″ x 3″ active area NaI (Tl) detector and nominal FWHM of 0.875 keV at 122 keV and 1.8 keV at 1.33 MeV. It is coupled to a Canberra DSA-1000 multichannel analyser with the Genie 2000 software package. Efficiency calibration of the system was performed using the Canberra LabSOCS package, based on the Monte Carlo method (Arnedo et al., 2017; Arriola-Velásquez et al., 2019; Guerra et al., 2017, 2015). Calibration was verified using reference standards for IAEA RGK-1 (potassium sulfate), RGU-1 (uranium ore) and RGTh-1 (thorium ore). Energy calibration was carried out using a 155Eu/22Na (Canberra ISOXSRCE, 7F06-9/10138 series) and confirmed using the 1460.8 keV line of ^{40}K (IAEA RGK-1) (Arnedo et al., 2017).

The radionuclides of interest were determined from different photopeaks. ^{226}Ra was determined from ^{214}Pb, using the 351.9 keV emission line. ^{210}Pb was directly measured using the 46.5 keV emission line. The activity concentration of ^{228}Ra was calculated from ^{228}Ac by the 911.2 keV emission line. Activity concentrations of ^{40}K and ^{137}Cs were directly measured using emission lines 1460.8 keV and 661.8 keV, respectively. The counting time for each sample was around 24 h.

In addition, ^{210}Pb is derived from the decay of ^{222}Rn (half-life of 3.8 days). This ^{222}Rn is a gas progeny of ^{226}Ra that partially diffuses into the atmosphere where it rapidly decays into ^{210}Pb. Then, this ^{210}Pb falls back to the earth's surface by wet and dry deposition. This deposited ^{210}Pb is not in equilibrium with its progenies ^{226}Ra and it is known as unsupported or excess $^{210}Pb_{ex}$ (Gaspar et al., 2017; Hülse and Bentley, 2012; Wakiyama et al., 2010). Thus, the activity of $^{210}Pb_{ex}$ was determined by the difference between the activity concentrations of ^{210}Pb and ^{226}Ra.

2.4. ICP-OES, ICP-MS and X-ray diffraction analysis

Inductively-coupled, plasma, optical emission spectrometry (ICP-OES) was used to carry out a multi-element analysis (Pozebon, 2002) of the samples and an inductively-coupled plasma mass spectrometry (ICP-MS) analysis was used to report the activity concentrations of uranium and thorium radioisotopes (Halliday et al., 1998; Walder and Freedman, 1992; Zheng et al., 2003) for each sample. The accuracy and repeatability of the results for both analyses were confirmed by using two reference materials (UREM-11 bulk sample of low-grade uranium ore and MESS-4 Beaufort Sea sediment) alongside the samples. Moreover, in the case of the ICP-MS analysis, a third reference material (IAEA-385 Irish sea sediment) was also used for method validation.

The ICP-MS instrument, as described in Pittauer et al. (2018), has a jet interface and uses an APEX-IR desolvation to maximize ion transmission of the samples. The effects of instrumental mass bias and uranium hybrid formation were controlled to make sure the results were clear of these effects. Furthermore, the results obtained for ^{238}U were not directly measured by the detector but calculated from the activity obtained for ^{235}U and the natural ratio $^{238}U/^{235}U$.

Finally, Powder X-ray diffraction (XRPD) data acquisition was carried out by an X'Pert PRO (PANalytical) Diffractometer, in θ-2θ Bragg-Brentano geometry, equipped with an X'Celerator LPS detector. The 5° to 80° 2θ range was investigated using CuKα radiation, working at 40 kV current tension, 40 mA current intensity and collecting at 0.02° steps, with a fixed divergence slit angle of 0.25°. Samples were ground on an agate mortar and then pressed in a back-load sample holder. The sample holder was spun during data acquisition. Diffraction patterns were analysed using X'Pert HighScore v. 2.1 (PANalytical©) software and mineral phases were matched using PDF2 (ICDD).

Selected grains of sample PLC18_8.2 were also checked by single crystal X-ray diffraction (SCXRD) using a Rigaku Oxford Diffraction XtaLAB Synergy diffractometer equipped with a PhotonJet (Mo) X-ray

Source, operating at 50 kV and 1 mA, and a Hybrid Pixel Array detector at 62 mm from the sample position. Intensity data was extracted from the images using CrysAlisPro 1.171.40.71a (Rigaku Oxford Diffraction, 2020). Crystal structures were refined using SHELX-2018 (Sheldrick, 2015) starting for atom coordinates collected from literature. Crystallographic information files including the results of these structure refinements are included in this paper as electronic supplementary material.

2.5. Proficiency test

In order to establish whether the measurements of radionuclides were optimal, the Analytical Laboratories for the Measurement of Environmental Radioactivity (ALMERA) proficiency test was performed (IAEA, 2011; Osvath et al., 2016; Shakhashiro et al., 2012). For this test, two parameters were calculated and, depending on the results of both parameters, the activity value given for one sample would be acceptable and/or different from the ones of another sample. First, the u-test was calculated following Eq. (1):

$$u_{test} = \frac{|A_A - A_B|}{\sqrt{u_A^2 + u_B^2}} \quad (1)$$

where A_A corresponds to the activity concentration value of one sample from the minimum activity concentration campaign, u_A is the uncertainty associated with that activity, A_B is the activity concentration value obtained for one sample from the same sampling point in the maximum activity concentration campaign and u_B is the uncertainty of that measurement. This u-test was performed with a limiting value to determine if a result passes the test of 2.58 for a 99% level of probability ($u_{test} < 2.58$). Therefore, when $u > 2.58$ the pair of values reported was significantly different.

On the other hand, to assess the uncertainty of the reported measurements, the P_{score} was calculated with the following equation:

$$P_{score} = \sqrt{\left(\frac{u_A}{A_A}\right)^2 + \left(\frac{u_B}{A_B}\right)^2} \quad (2)$$

where A_A corresponds to the activity concentration value of one sample from the minimum activity concentration campaign, u_A is the uncertainty associated with that activity, A_B is the activity concentration value obtained for the samples corresponding to the same sampling point in the maximum activity concentration campaign and u_B is the uncertainty of that measurement. According to this test, when the P_{score} < Limit of Acceptable Precision (LAP), the results give scores that are acceptable for the claimed uncertainty. The LAP values used in the evaluation of P_{score} correspond to the values given in IAEA (2011) of 20% for all of the radionuclides analysed in this study.

2.6. Statistical analysis

First, a correlation analysis between the meteorological, oceanographic and radioactivity data was performed. Then, different statistical tests were performed with the activity concentration of the different radionuclides of interest divided into groups established by the environmental conditions. Levene's test (Schultz, 1985) was carried out to evaluate the homogeneity of the variance. After that, a one-way ANOVA test was performed to evaluate the presence of significant differences among the different groups. Finally a Tukey's Honestly Significant Difference (HSD) Test (Williams and Abdi, 2010) was used to establish the exact groups within which significant differences were found.

3. Results and discussion

3.1. Activity concentrations

A Shapiro-Wilk test (Shapiro and Wilk, 1965) was carried out for each time series of the values of activity concentration (for ^{226}Ra, ^{228}Ra, ^{40}K and $^{210}Pb_{ex}$) corresponding to each sampling point (360 data for each radionuclide). For all of the results, the data showed a normal distribution at a significance level of 0.05, except for the values in the series of ^{40}K for sampling points P1 and P2. For these sampling points, normality was found at a significance level of 0.01. The boxplot in Fig. 2 shows the activity concentration of ^{226}Ra, ^{228}Ra, ^{40}K and $^{210}Pb_{ex}$ for each sampling point during the whole study period. The activity concentration of ^{226}Ra ranged from 4.6 ± 0.7 to 24.9 ± 1.5 Bq kg^{-1} with a mean value of 13.3 ± 0.9 Bq kg^{-1}. In the case of ^{228}Ra, the activity concentration values were reported between 4.7 ± 1.3 and 33.3 ± 2.9 Bq kg^{-1} with a mean value of 17.0 ± 1.6 Bq kg^{-1}. Regarding ^{40}K, activity concentration values fluctuated from below the detection limit of 4 Bq kg^{-1} (BDL) to 842 ± 37 Bq kg^{-1} with a mean value of 405 ± 19 Bq kg^{-1}. Finally, $^{210}Pb_{ex}$ varied from 11.3 ± 3.8 to 65.9 ± 6.8 Bq kg^{-1} with a mean value of 32.7 ± 5.7 Bq kg^{-1}.

The data shows similar behaviour to that in the work of Arriola-Velásquez et al. (2019). There were, generally, lower activities in sampling points in the southern arch, the area being fully open to wave action, and a progressive increase of the activity concentration of ^{226}Ra, ^{228}Ra and ^{40}K in the northern arch, the area protected by the offshore rocky bar. The $^{210}Pb_{ex}$ reports the same behaviour as in the previous study, with similar activity concentration values found along the beach. This reinforces the conclusions found in that work and enhances the proposed idea of the use of the distribution of ^{226}Ra, ^{228}Ra and ^{40}K as tracers of marine sediment dynamics due to its distribution along the beach, conditioned by the morphology of the natural offshore rocky bar. Furthermore, the results of this study were analysed from the perspective of the three zones of activity distribution along the beach that appeared in the study of 2019, i.e. an area totally exposed to the wave interactions (zone I), an area located in front of the openings of the offshore rocky bar (zone II) and an area fully protected against wave action (zone III).

Additionally, the temporal series for the mean values of ^{226}Ra, ^{228}Ra, ^{40}K and the ratio ^{226}Ra/^{228}Ra for each of the zones of the beach are shown in Fig. 3. In zone I, ^{226}Ra, ^{228}Ra and ^{40}K follow a similar pattern with maxima activity concentration values mostly seen in the summer months, with some exceptions, and lower activity concentration values in winter months. For zone II, some alternations of maxima and minima activity concentration values appear. In the case of zone III, the three radionuclides show similar behaviour with rather constant activity concentrations for the whole study region. This seems to be tracing what is described in the literature about the sedimentary transport and budget in Las Canteras beach (Alonso, 1994, 1993; Alonso and Vilas, 1996). According to this, during erosion periods, the open part of the beach (zone I in this study) loses a large amount of sand that is transported lengthwise to the closed part of the beach (zone III in this study), while, during accumulation periods, there is an input of sediments to the open part of the beach. The erosion periods would occur when a storm event hits the beach, which would be more likely to occur in winter. Therefore, the maximum and minimum activity concentration values found for ^{226}Ra, ^{228}Ra an ^{40}K in zone I seem to be tracing the input and output of sand in this part of the beach during the different periods. In the case of zone III, the literature explains that this part is in a constant accumulation period, so that could explain the constant activity concentration values found for this part. In comparison to these radionuclides, $^{210}Pb_{ex}$ does not show much of a difference for the whole study period, except for the activity concentration of September 2017 in zone I that is slightly higher to the rest. This reinforces the idea that the agents controlling the changes in $^{210}Pb_{ex}$ are different from the ones controlling the distribution of the other radionuclides studied (Arriola-Velásquez et al., 2019).

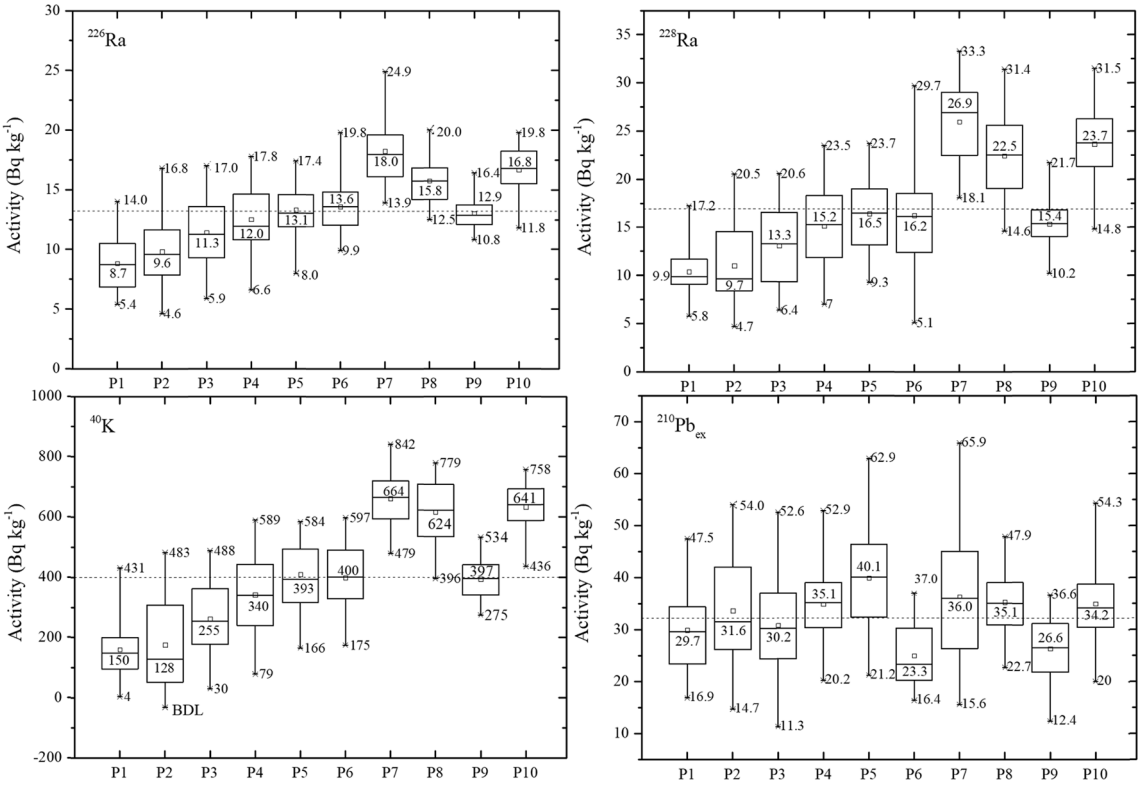

Fig. 2. Boxplots of the activity concentrations found for each sampling point for ^{226}Ra, ^{228}Ra, ^{40}K and ^{210}Pb$_{ex}$. The dash line indicates the mean activity concentration value. The numbers that appear in each whisker correspond to the maximum and minimum activity concentration values. The number in the middle indicates the mean activity concentration value for each sampling point.

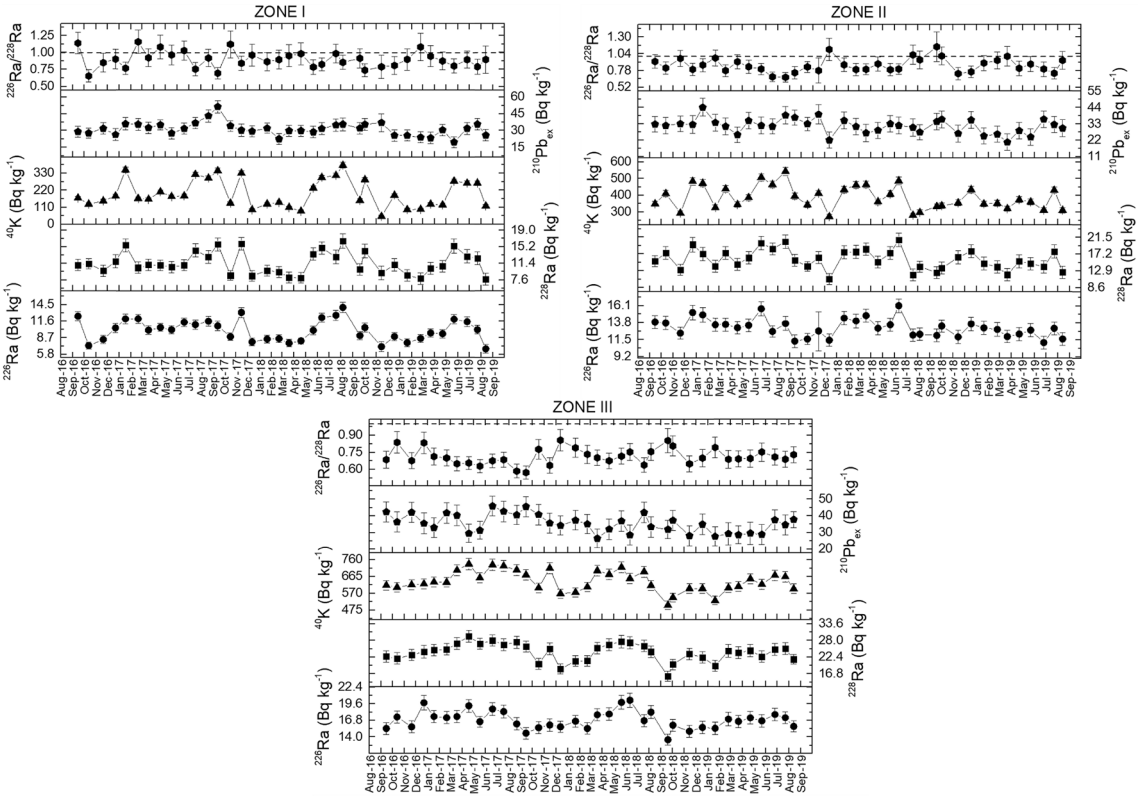

Fig. 3. Temporal series of the activity concentration of ^{226}Ra, ^{228}Ra, ^{40}K, ^{210}Pb$_{ex}$ and the ratio ^{226}Ra/^{228}Ra during the study period for the different zones established in (Arriola-Velásquez et al., 2019) for Las Canteras beach.

Thus, $^{210}Pb_{ex}$ does not seem to be a good tracer of marine sediment dynamics, while ^{226}Ra, ^{228}Ra and ^{40}K seem to be good candidates for tracing erosion and accumulation periods.

Finally, the results for $^{226}Ra/^{228}Ra$ show different things in the different zones. According to what was suggested for this ratio in the literature (Dai et al., 2011), when this ratio was below 1, it would indicate an accumulation period. On the other hand, values above 1 would indicate an erosion period. In Fig. 3, the limit is marked with a dashed line and it can be appreciated that for zone III, all of the values are below 1. This would indicate a constant accumulation period, which agrees with what is described in the literature for the closed part of the beach. However, in zones I and II the results are not so conclusive and clear differences do not appear between summer and winter months. In the work of Dai et al. (2011) the use of this ratio was based on the presence of clay minerals in the study region. The northeastern part of El Confital bay, where the northern arch of the beach (zone III) is located, is

Table 1
Correlation coefficients matrix of activity concentration of ^{226}Ra, ^{228}Ra, ^{40}K, $^{210}Pb_{xc}$, the ratio $^{226}Ra/^{228}Ra$, wave approach direction, significant wave height (H_S), wind approach direction, wind speed, PM_{10}, temperature (T), relative humidity (RH) and atmospheric pressure (PRB) for A) Zone I, B) Zone II and C) Zone III. The p-value is set at 0.05.

(A) ZONE I	Wave approach direction	H_S (m)	Wind approach direction	Wind speed (m s^{-1})	PM_{10}	T (°C)	RH (%)	PRB (mb)	^{226}Ra	^{228}Ra	^{40}K	$^{210}Pb_{ex}$	$^{226}Ra/^{228}Ra$
Wave aproach direction	1	*0.516*	*0.230*	*0.386*	*0.996*	*0.545*	*0.515*	*0.869*	*0.020*	*0.016*	*0.005*	*0.326*	*0.683*
H_S (m)	0.112	1	*0.087*	*0.000*	*0.579*	*0.009*	*0.280*	*0.059*	*0.000*	*0.000*	*0.000*	*0.035*	*0.294*
Wind aproach direction	0.205	−0.290	1	*0.074*	*0.611*	*0.038*	*0.950*	*0.016*	*0.744*	*0.625*	*0.479*	*0.245*	*0.381*
Wind speed	−0.149	0.584	−0.301	1	*0.451*	*0.059*	*0.277*	*0.078*	*0.318*	*0.108*	*0.038*	*0.017*	*0.162*
PM_{10}	0.001	0.096	−0.088	0.130	1	*0.090*	*0.000*	*0.341*	*0.803*	*0.965*	*0.657*	*0.953*	*0.624*
T (°C)	−0.104	−0.429	0.347	−0.318	0.287	1	*0.175*	*0.016*	*0.149*	*0.103*	*0.025*	*0.029*	*0.764*
RH (%)	−0.112	−0.185	−0.011	−0.186	−0.626	−0.231	1	*0.450*	*0.757*	*0.580*	*0.493*	*0.635*	*0.510*
PRB (mb)	0.028	0.318	−0.398	0.297	0.163	−0.398	−0.130	1	*0.206*	*0.124*	*0.181*	*0.249*	*0.508*
^{226}Ra	−0.385	−0.603	−0.056	−0.171	0.043	0.245	0.053	−0.216	1	*0.000*	*0.000*	*0.068*	*0.662*
^{228}Ra	−0.399	−0.633	0.084	−0.272	0.008	0.276	0.095	−0.261	**0.797**	1	*0.000*	*0.019*	*0.001*
^{40}K	−0.457	−0.688	0.122	−0.347	0.077	0.373	0.118	−0.228	**0.824**	**0.940**	1	*0.003*	*0.023*
$^{210}Pb_{ex}$	−0.168	−0.352	0.199	−0.394	−0.010	0.363	0.082	−0.197	0.308	0.390	0.477	1	*0.318*
$^{226}Ra/^{228}Ra$	0.071	0.180	−0.150	0.238	0.085	−0.052	−0.113	0.114	0.075	**−0.517**	−0.378	−0.171	1
p-value 0.05													

(B) ZONE II	Wave approach direction	H_S (m)	Wind approach direction	Wind speed (m s^{-1})	PM_{10}	T (°C)	RH (%)	PRB (mb)	^{226}Ra	^{228}Ra	^{40}K	$^{210}Pb_{ex}$	$^{226}Ra/^{228}Ra$
Wave aproach direction	1	*0.516*	*0.230*	*0.386*	*0.996*	*0.545*	*0.515*	*0.869*	*0.864*	*0.867*	*0.488*	*0.918*	*0.753*
H_S (m)	0.112	1	*0.087*	*0.000*	*0.579*	*0.009*	*0.280*	*0.059*	*0.338*	*0.087*	*0.117*	*0.010*	*0.143*
Wind aproach direction	0.205	−0.290	1	*0.074*	*0.611*	*0.038*	*0.950*	*0.016*	*0.648*	*0.117*	*0.138*	*0.374*	*0.051*
Wind speed	−0.149	0.584	−0.301	1	*0.451*	*0.059*	*0.277*	*0.078*	*0.572*	*0.436*	*0.556*	*0.070*	*0.114*
PM_{10}	0.001	0.096	−0.088	0.130	1	*0.090*	*0.000*	*0.341*	*0.837*	*0.500*	*0.808*	*0.864*	*0.310*
T (°C)	−0.104	−0.429	0.347	−0.318	0.287	1	*0.175*	*0.016*	*0.076*	*0.840*	*0.615*	*0.413*	*0.515*
RH (%)	−0.112	−0.185	−0.011	−0.186	−0.626	−0.231	1	*0.450*	*0.280*	*0.476*	*0.521*	*0.860*	*0.876*
PRB (mb)	0.028	0.318	−0.398	0.297	0.163	−0.398	−0.130	1	*0.215*	*0.968*	*0.981*	*0.466*	*0.357*
^{226}Ra	0.030	−0.165	0.079	0.097	−0.036	−0.299	−0.185	0.212	1	*0.000*	*0.000*	*0.143*	*0.085*
^{228}Ra	−0.029	−0.289	0.266	−0.134	−0.116	−0.035	−0.123	−0.007	**0.764**	1	*0.000*	*0.024*	*0.000*
^{40}K	−0.119	−0.266	0.252	−0.102	−0.042	−0.087	−0.111	0.004	**0.744**	**0.950**	1	*0.011*	*0.000*
$^{210}Pb_{ex}$	−0.018	−0.424	0.153	−0.305	−0.030	0.141	−0.030	0.126	0.249	0.375	0.420	1	*0.056*
$^{226}Ra/^{228}Ra$	0.054	0.249	−0.328	0.268	0.174	−0.112	0.027	0.158	−0.291	**−0.804**	**−0.731**	−0.322	1
p-value 0.05													

(C) ZONE III	Wave approach direction	H_S (m)	Wind approach direction	Wind speed (m s^{-1})	PM_{10}	T (°C)	RH (%)	PRB (mb)	^{226}Ra	^{228}Ra	^{40}K	$^{210}Pb_{ex}$	$^{226}Ra/^{228}Ra$
Wave aproach direction	1	*0.516*	*0.230*	*0.386*	*0.996*	*0.545*	*0.515*	*0.869*	*0.538*	*0.188*	*0.112*	*0.608*	*0.264*
H_S (m)	0.112	1	*0.087*	*0.000*	*0.579*	*0.009*	*0.280*	*0.059*	*0.194*	*0.042*	*0.025*	*0.461*	*0.165*
Wind aproach direction	0.205	−0.290	1	*0.074*	*0.611*	*0.038*	*0.950*	*0.016*	*0.138*	*0.157*	*0.181*	*0.233*	*0.685*
Wind speed	−0.149	0.584	−0.301	1	*0.451*	*0.059*	*0.277*	*0.078*	*0.875*	*0.114*	*0.118*	*0.160*	*0.013*
PM_{10}	0.001	0.096	−0.088	0.130	1	*0.090*	*0.000*	*0.341*	*0.906*	*0.964*	*0.343*	*0.343*	*0.991*
T (°C)	−0.104	−0.429	0.347	−0.318	0.287	1	*0.175*	*0.016*	*0.853*	*0.218*	*0.232*	*0.043*	*0.191*
RH (%)	−0.112	−0.185	−0.011	−0.186	−0.626	−0.231	1	*0.450*	*0.297*	*0.286*	*0.698*	*0.406*	*0.610*
PRB (mb)	0.028	0.318	−0.398	0.297	0.163	−0.398	−0.130	1	*0.512*	*0.020*	*0.006*	*0.424*	*0.022*
^{226}Ra	−0.106	−0.221	0.252	0.027	0.020	0.032	−0.179	−0.113	1	*0.000*	*0.000*	*0.584*	*0.995*
^{228}Ra	−0.225	−0.341	0.241	−0.268	−0.008	0.211	−0.183	−0.387	**0.675**	1	*0.000*	*0.455*	*0.000*
^{40}K	−0.270	−0.374	0.228	−0.265	−0.163	0.204	−0.067	−0.453	**0.587**	**0.915**	1	*0.107*	*0.000*
$^{210}Pb_{ex}$	−0.088	−0.127	0.204	−0.239	−0.163	0.340	−0.143	−0.137	−0.094	0.128	0.273	1	*0.143*
$^{226}Ra/^{228}Ra$	0.191	0.236	−0.070	0.410	−0.002	−0.223	0.088	0.380	0.001	**−0.726**	**−0.687**	−0.249	1
p-value 0.05													

the only part where clay minerals have been found in previous studies of the region (Mangas and Julià-Miralles, 2015). Therefore, This could explain why the ratio seems to work in the protected part of Las Canteras beach (i.e. the northern part) but does not seem to work so well for the other two parts to the south. Thus, further analysis of this ratio is necessary to evaluate its precision in tracing erosion and accumulation periods for the whole beach.

3.2. Analysis of the relationships between environmental variables and activity concentration changes

Aerosols and atmospheric parameters are known to be correlated with the transport of natural radionuclides such as ^{40}K and $^{210}Pb_{ex}$ (Dueñas et al., 2017; Karlsson et al., 2008; López-Pérez et al., 2013). Moreover, studies in the Canary Islands have found correlations between the deposition of materials floating in the sea, such as plastic debris, wave approach direction and the significant wave height (Herrera et al., 2018). Therefore, correlation analysis was carried out between the mean activity concentration values found during the whole study period for ^{226}Ra, ^{228}Ra, ^{40}K and $^{210}Pb_{ex}$ and the ratio $^{226}Ra/^{228}Ra$ in the different zones of the beach, as well as the atmospheric and marine parameters described in section 2 of this work. The results are shown in Table 1. The p-value obtained for each correlation coefficient is also represented, and is statistically significant when p-values < 0.05. However, when a p-value was < 0.05, but the correlation coefficient was below 0.5, no correlation was considered. Moreover, a strong correlation was considered when p-value < 0.005 and the correlation coefficient was >0.6.

All three zones presented a strong correlation in the activity concentration of ^{226}Ra, ^{228}Ra and ^{40}K between each other, while no correlation was found with the activity concentration of $^{210}Pb_{ex}$. This supports the hypothesis that the agents controlling the distribution of the first three radionuclides are different from the ones controlling the distribution of unsupported ^{210}Pb. Furthermore, zone I only presented an inverse correlation between the activity concentration of ^{226}Ra, ^{228}Ra and ^{40}K and the significant wave height. This indicates that, when there is a higher significant wave height, higher waves hit the beach and the activity concentration of those radionuclides is lower. According to the literature (Alonso, 2005, 1994, 1993; Alonso and Vilas, 1996), when a big storm event hits the southern arch of the beach, where all sampling points from zone I are located, there is a loss of sediment from the beach, that is transported lengthwise to the northern arch. On the contrary, when there is an accumulation period, the amount of sediments in the southern arch increases, as well as in the northern arch. The northern part is protected by the natural offshore rocky bar and is in a constant accumulation period. This sedimentary behaviour seems to agree with what occurs with natural radionuclide concentrations in zone I, when facing large significant wave heights, normally related to storm events. In zones II and III, the activity concentration of the different radionuclides did not show any correlation with any of the atmospheric or marine parameters either but still presented correlations among ^{226}Ra, ^{228}Ra and ^{40}K. The results for zones II and III (the areas that are in front of the natural offshore rocky bar and its openings) are what would be expected. According to the literature (Medina et al., 2006), the wave approach direction suffers diffraction when waves hit the bar and its openings, creating internal currents between the bar and the beach line. Therefore, it would be expected that the data obtained from a buoy outside El Confital Bay would not present any correlation with the activity concentration values in these two areas. Thus, these internal currents should be further studied to better understand the behaviour of natural radionuclide distributions associated with the sediments in the closed and semi-closed parts of the beach. In the case of $^{210}Pb_{ex,}$ no correlation was found with any of the atmospheric or marine parameters in any of the three zones. Therefore, this element was no longer considered in the rest of this study.

Regarding the $^{226}Ra/^{228}Ra$ ratio, all three zones presented an inverse correlation with the activity concentration of ^{228}Ra, showing a higher correlation in zones II and III. This means that when the activity concentration of ^{228}Ra was higher the ratio would be lower. The use of this ratio as an indicator of erosion and accumulation periods in the work of Dai et al. (2011) was based on the higher mobility of ^{228}Ra against ^{226}Ra in the crystal framework of clay minerals. According to their study, during erosion periods the ratio would be higher due to the loss of ^{228}Ra and during accumulation periods the ratio would be lower due to the higher input of ^{228}Ra contained in the clay minerals of the sediments. For Las Canteras beach, clay minerals have been found in the north-northeast part of El Confital Bay where the protected area of Las Canteras beach is located (Mangas and Julià-Miralles, 2015). This could explain why the correlation is stronger for zones II and III since those are the areas closest to where clay minerals were found. In addition, for zones II and III the correlation analysis also points out an inverse correlation between the ratio and ^{40}K. In previous studies it has been found that clay materials have activity concentration values of ^{40}K one order of magnitude higher than the activity concentration values of ^{232}Th (the parent radionuclide of ^{228}Ra) and ^{226}Ra (Hewamanna et al., 2001; Raghu et al., 2020). This differences in activity concentration values seems to agree to with the results obtained for ^{226}Ra, ^{228}Ra and ^{40}K in Las Canteras beach for the area where clay minerals are present (northern part of the beach). Moreover, the sediment dynamics described in literature for Las Canteras beach explains that during erosion periods there is a lengthwise transport of sediment from the southern arch to the northern arch. On the contrary, during accumulation periods a sediment transport from the northern arch to the south part of the beach occurs (Alonso, 2005, 1993; Alonso and Vilas, 1996). Therefore, the presence of the clay minerals that were reported in the work of Mangas and Julià-Miralles, (2015) and its movement along the beach during erosion and accumulation periods could explain the inverse correlation between the ratio $^{226}Ra/^{228}Ra$ and the activity concentration values of ^{228}Ra and ^{40}K, since these clay minerals could be transporting both radionuclides. This seems to point out the role these radionuclides have as tracers of the transport of sand along the beach during erosion and accumulation periods. However, it is important to mention that some petrographic studies also show that feldspars tend to accumulate in the northern part of the beach (Alonso and Pérez Torrado, 1992). Thus, these minerals could also be contributing to the changes in ^{40}K. In addition, the ratio did not have any correlation with the activity concentration of ^{226}Ra, and thus only the presence of clay minerals in the northern part of the beach could not justify the changes observed for ^{226}Ra, ^{228}Ra and ^{40}K during erosion and accumulation periods in the whole beach. Hence, the ratio does not seem to be a suitable tracer for the sediment dynamics of the whole beach.

The results of the correlation analysis are shown as azimuth plots in Fig. 4. These plots represent the variation of activity concentration of ^{226}Ra, ^{228}Ra and ^{40}K according to the wave approach direction and the significant wave height in each campaign. It can be appreciated how, for zone I, the activity concentration values seemed to be higher when the significant wave height was smaller. In the cases of zones II and III, this pattern does not appear, which could again be related to the fact that these two areas are protected by the natural offshore rocky bar. The azimuth plots for the ratio $^{226}Ra/^{228}Ra$ are also presented in Fig. 5 but no pattern seems to appear. The results of the ANOVA and the Tukey's test that appear in Table 2 confirm what was observed in the azimuth plots. The ANOVA test for a prob-F level of 0.05 pointed out that for zone I there were significant differences in the different groups established for each radionuclide based on the significant wave height. The Tukey's test with a p-value of 0.05 showed that these differences were indeed between the groups of lower wave height and higher and medium wave height. As explained previously, the literature indicates that big storm events erode the sediments in the southern arch of Las Canteras beach since it is totally exposed to the wave action. Therefore, if the radionuclides used in this study show a similar pattern, when high, significant wave heights hit that part of the beach, it seems that these radionuclides are, indeed, tracing the sediment dynamics of the beach. Thus, its role as

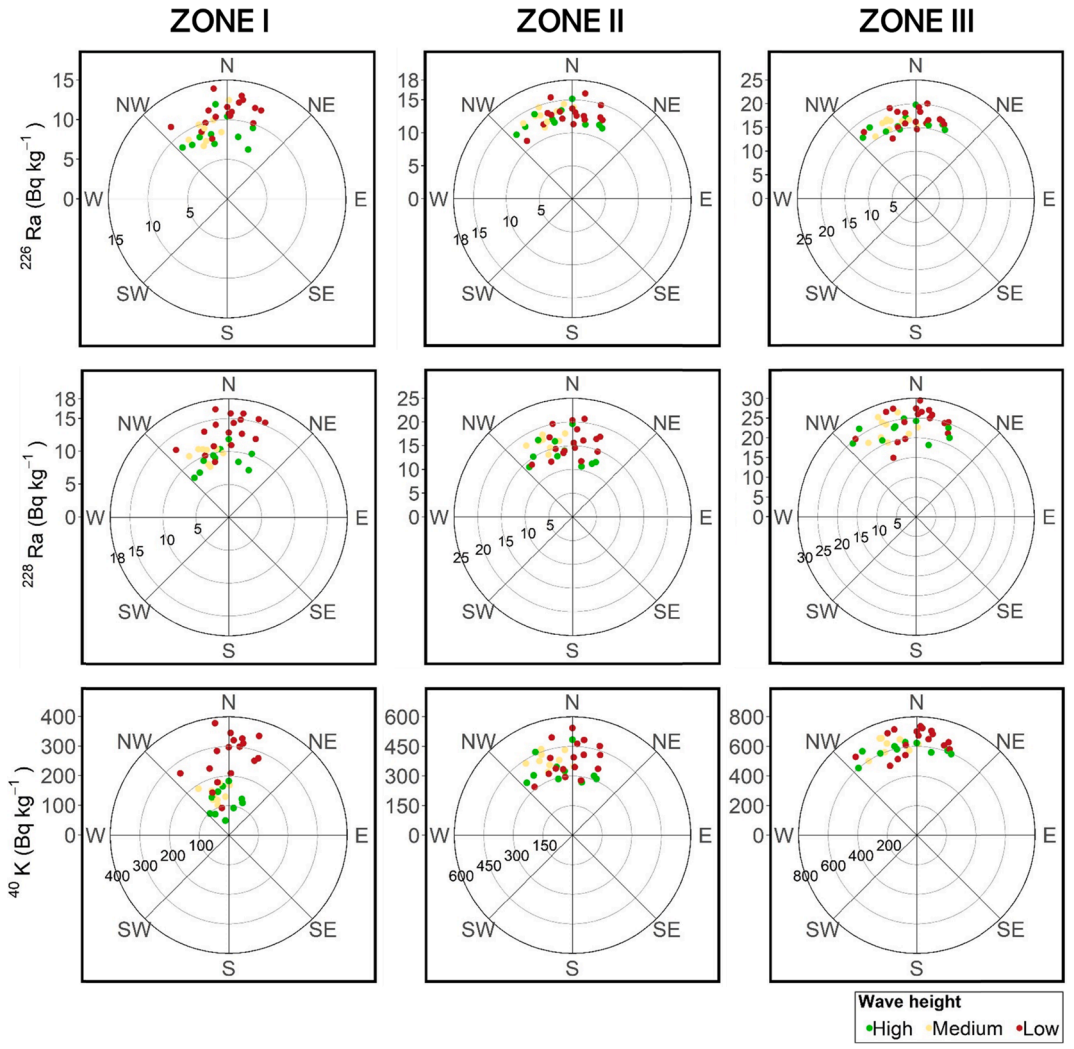

Fig. 4. Azimuth plot of wave height and direction and activity concentration of ^{226}Ra, ^{228}Ra and 40 K for the different zones in Las Canteras beach.

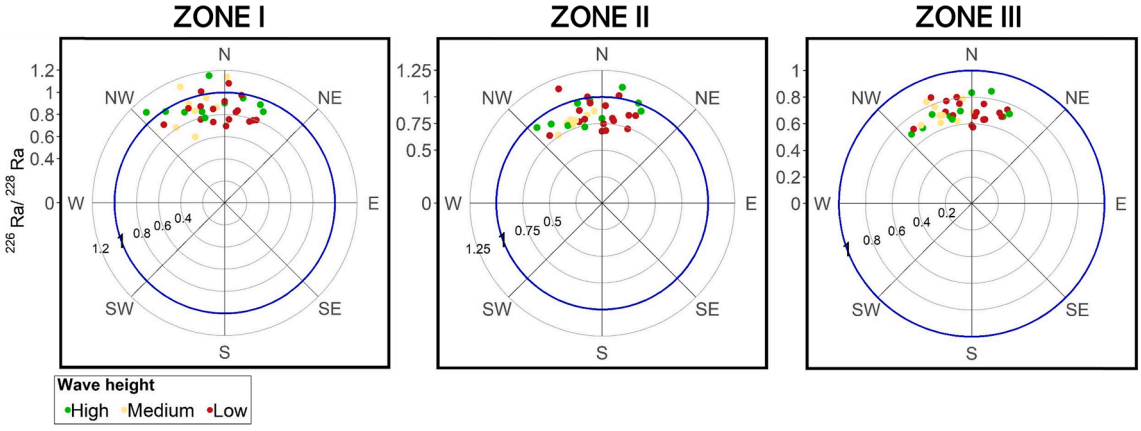

Fig. 5. Azimuth plot of wave height and direction and activity concentration of the ratio ^{226}Ra/ ^{228}Ra. In blue is marked the limit of 1. (For interpretation of the references to colour in this figure legend, the reader is referred to the web version of this article.)

a tracer of these dynamics can be confirmed. In zones II and III, no significant differences were found. This could be related to the protection against wave action that the offshore rocky bar offers to the sampling points in these two zones.

The results relating to wave approach direction also reported significant differences between the campaigns where the wave approach direction was NE and those when it was NW, in zone I. Since this behaviour was not clear in the azimuth plots, the boxplots of Fig. 6 were made. It represents the activity concentration values of ^{226}Ra (Fig. 6a), ^{228}Ra (Fig. 6b) and ^{40}K (Fig. 6c) for the campaigns with NE and NW wave approach directions. It shows that, in campaigns with a NE wave approach direction, the activity concentration values of these elements

Table 2
One-way ANOVA test for the identification of the presence of significant differences in the temporal series of ^{226}Ra, ^{228}Ra. ^{40}K and the ratio $^{226}Ra/^{228}Ra$ for the different campaigns in the different zones of Las Canteras beach. The result of the p-value for the Tukey's test is also displayed to identify the groups that present significant differences between them.

Area	Field	F	Prob-F	Tuckey's test
ZONE I				
^{226}Ra	Significant wave height	9.61900	0.0005110	Low-high (0.0009) Low-medium (0.0114)
	Wave direction	6.02300	0.0194000	NW-NE (0.0194)
^{228}Ra	Significant wave height	19.14000	0.0000030	Low-High (0.0000065) Low- Medium (0.0004618)
	Wave direction	6.67200	0.0143000	NW-NE (0.0142665)
^{40}K	Significant wave height	25.34000	0.0000002	Low-High (0.0000008) Low- Medium (0.0000358)
	Wave direction	9.12100	0.0047700	NW-NE (0.0047708)
$^{226}Ra/^{228}Ra$	Significant wave height	1.98000	0.1540000	–
	Wave direction	0.21400	0.6470000	–
ZONE II				
^{226}Ra	Significant wave height	0.73900	0.4850000	–
	Wave direction	0.02600	0.8720000	–
^{228}Ra	Significant wave height	1.97400	0.1550000	–
	Wave direction	0.01300	0.9100000	–
^{40}K	Significant wave height	1.58700	0.2200000	–
	Wave direction	0.41700	0.5230000	–
$^{226}Ra/^{228}Ra$	Significant wave height	1.66000	0.2060000	–
	Wave direction	0.05400	0.8180000	–
ZONE III				
^{226}Ra	Significant wave height	0.63300	0.5370000	–
	Wave direction	0.35700	0.5540000	–
^{228}Ra	Significant wave height	0.98400	0.3850000	–
	Wave direction	1.64500	0.2080000	–
^{40}K	Significant wave height	1.72000	0.1950000	–
	Wave direction	2.41200	0.1300000	–
$^{226}Ra/^{228}Ra$	Significant wave height	0.22000	0.8040000	–
	Wave direction	1.16300	0.2890000	–

ANOVA prob-F 0.05.
Tuckey's test p-value 0.05.

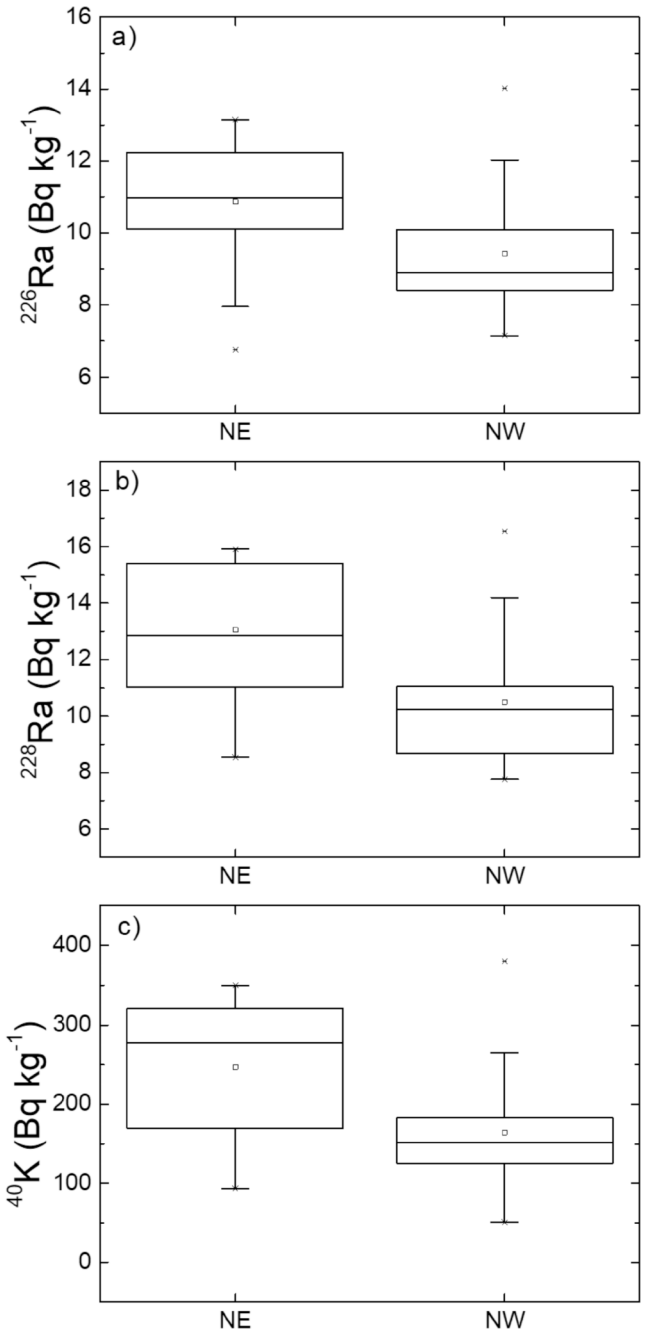

Fig. 6. Boxplot of the activity concentrations obtained for zone I in each campaign for each of the wave approach directions. (a) ^{226}Ra, (b) ^{228}Ra and (c) ^{40}K.

were higher. The NE part of the bay and the north part of the beach is where the clay minerals and feldspars were found (Alonso and Pérez Torrado, 1992; Mangas and Julià-Miralles, 2015). Therefore, the results point to the possible influence of the minerals located in the northern part of the beach, in the changes of activity concentration values found in zone I during the whole study period. In this case, zones II and III did not show any significant differences either.

Regarding the ratio $^{226}Ra/^{228}Ra$, no significant differences were found for any of the three zones. According to the literature (Alonso, 2005, 1993; Alonso and Vilas, 1996) the area fully protected by the natural offshore rocky bar (zone III) is in a constant accumulation period. Moreover, zone II is also protected by the bar, so the lack of significant differences can be expected in these two parts of the beach. However, although the absence of significant differences in zones II and III could be explained due to the presence of the bar, this would not justify what happens in zone I. Clay minerals are not the only minerals that could contain ^{228}Ra and ^{40}K. Therefore, despite the fact that it seemed to work well in previous studies as a tracer of erosion and accumulation periods (Arriola-Velásquez et al., 2019; Dai et al., 2011), these ratios might not be completely suitable as a tracer for marine sediment dynamics in Las Canteras beach. Instead, the results suggest that ^{226}Ra, ^{228}Ra and ^{40}K are more suitable tracers of the sediment dynamics of the beach.

3.3. ICP-MS, multi-element and mineralogical analysis

The maximum gamma activity campaign (August 2018) was considered an accumulation campaign and the minimum gamma activity campaign (November 2018) an erosion one. Thus, 3 samples were selected from the accretion campaign and 3 samples were selected from

the erosion campaign. These 6 samples were studied to further comprehend the variations in the radioactivity, chemical and mineralogy composition of the beach sand during erosion and accumulation periods. Moreover, out of the 3 samples from each campaign 2 belonged to sampling stations P1 and P2 and the third one to sampling station P8 (Fig. 1.). Sampling stations P1 and P2 belong to the open part of the beach so the results of these stations would give clearer information about erosion and accumulation periods since that part is the one more affected by the different seasons. In contrast, sampling station P8 belongs to the protected part of the beach. This sampling station is in a constant accumulation period and, therefore, not many changes should be expected in its composition during erosion and accumulation seasons. By choosing these 6 samples it was expected to better understand the role of natural radionuclides as a tracers of sedimentary dynamics in Las Canteras beach.

In Table 3, the results for the activity concentration values found in each sample for ^{235}U, ^{238}U, ^{234}U, ^{230}Th and ^{232}Th by ICP-MS are shown, as well as the activity concentration values of ^{226}Ra, ^{228}Ra and ^{40}K found by gamma spectrometry. The results seem to present higher values of activity concentration in sampling points P1 and P2 in August 2018, than in November 2018, while sampling point P8 seems to stay quite stable for all activity concentration values in both campaigns. The results of the proficiency test (IAEA, 2011; Osvath et al., 2016; Shakhashiro et al., 2012) are also given in Table 3. In the case of sample PLC18_11.2 (corresponding to sampling point 2), the activity of ^{40}K was below the detection limit (BDL). Thus, the u_{test} and the P_{score} values were calculated using half of the minimum activity detectable, as an activity concentration value of that sample.

These results show that samples from sampling points P1 and P2, corresponding to zone I, present significant differences for the activity concentrations of all radionuclides. On the contrary, the samples from sampling point P8 in zone III did not present significant differences for almost any radionuclide, except for ^{235}U and ^{238}U. However, ^{238}U is calculated from the ^{235}U value and the natural ratio ^{238}U/^{235}U, so this explains why both present the same values in the proficiency test. Therefore, this means that the primordial uranium isotopes ^{235}U and ^{238}U are the only radionuclides that actually differ between one sample and the other. According to the literature (Alonso, 2005, 1994, 1993; Alonso and Vilas, 1996), the northern arch of Las Canteras beach is in a constant accumulation period, while the southern arch is the one that suffers variability in the loss and accumulation of sediments. Sampling points 1 and 2 are located in zone I, which is the area totally exposed to the wave action, while sampling point 8 is located in zone III in the northern arch, in the area protected by the offshore rocky bar. Therefore, it makes sense that samples from zone I present significant differences between the maximum and minimun activity concentration campaigns, whereas the sample from zone III does not have such differences. These results mean that, over time, there is a variation between maximum and minimum activity concentration in the area totally exposed to the wave action and, thus, these radionuclides could be good tracers for marine sediment dynamics in the open beach. Considering the activity concentration values of ^{232}Th, ^{228}Ra, ^{230}Th and ^{226}Ra obtained for all samples, if the ratios ^{232}Th/^{228}Ra and ^{230}Th/^{226}Ra were calculated, all of them would be approximately 1. This means that both Ra radioisotopes would be in equilibrium with their parents and, thus, their activity is also controlled by their parent radionuclides. Therefore, the parent radionuclides could also be following the same marine sediment dynamics and be used as tracers of the beach sediment dynamics.

In order to better understand the geochemical composition of the sediments transported along Las Canteras beach, a multi-element analysis and mineralogical analysis were carried out on the same six samples that were chosen for the ICP-MS analysis. The results of the multielement analysis for total rock composition of Ba, Ca, Mg and K are shown in Table 4. Total potassium was analysed to evaluate if similar

Table 4
Multielement analysis of the total rock composition of each sand sample. Concentrations given in g kg-1 of Ba, Ca, Mg and K were analyzed.

Sample	Ba	Ca	Mg	K
LOD of detector	0.0002	0.0552	0.0034	0.0203
LOB	0.0113	3.1764	0.384	0.109
LOD of the method	0.0226	6.3529	0.7681	0.2181
LOQ	0.0435	11.9209	1.4904	0.4227
PLC18_8.1	0.3176 ± 0.0005	192 ± 1	23.29 ± 0.30	13.13 ± 0.06
PLC18_8.2	0.3611 ± 0.0047	172 ± 2	22.21 ± 0.24	16.03 ± 0.10
PLC18_8.8	0.3805 ± 0.0023	167 ± 1	15.48 ± 0.09	21.69 ± 0.06
PLC18_11.1	0.1579 ± 0.0013	141 ± 1	66.80 ± 0.63	2.30 ± 0.02
PLC18_11.2	0.0519 ± 0.0005	25 ± 0	36.18 ± 0.18	0.65 ± 0.01
PLC18_11.8	0.3484 ± 0.0021	163 ± 1	14.58 ± 0.12	22.27 ± 0.08

Table 3
Activity concentrations in Bq kg^{-1} found for radionuclides ^{235}U, ^{238}U, ^{234}U, ^{230}Th and ^{232}Th measured by ICP-MS measurement and for ^{226}Ra, ^{228}Ra and ^{40}K measured by gamma spectrometry. In addition, the results of the proficiency test parameter u_{test} and P_{score} described in IAEA (2011), Osvath et al. (2016), Shakhashiro et al. (2012).

Sample	Sampling point	Date	^{235}U	^{238}U*	^{234}U	^{230}Th	^{232}Th	^{226}Ra	^{228}Ra	^{40}K
PLC18_8.1	P1	August 2018	0.717 ± 0.003	15.58 ± 0.06	16.92 ± 0.23	14.50 ± 0.87	14.81 ± 1.91	14.01 ± 0.95	17.23 ± 1.80	431 ± 20
PLC18_8.2	P2	August 2018	0.841 ± 0.004	18.27 ± 0.10	19.27 ± 0.19	17.88 ± 1.06	21.41 ± 1.94	16.81 ± 1.00	20.45 ± 1.79	483 ± 22
PLC18_8.8	P8	August 2018	0.906 ± 0.006	19.68 ± 0.12	20.64 ± 0.20	17.94 ± 0.47	22.99 ± 1.89	16.35 ± 1.05	24.45 ± 1.89	606 ± 27
PLC18_11.1	P1	November 2018	0.348 ± 0.003	7.56 ± 0.06	8.25 ± 0.13	8.60 ± 0.89	8.16 ± 0.91	6.30 ± 0.53	7.37 ± 0.95	81 ± 6
PLC18_11.2	P2	November 2018	0.388 ± 0.004	8.43 ± 0.08	9.44 ± 0.17	9.08 ± 0.62	8.43 ± 0.11	9.19 ± 1.36	9.38 ± 2.45	BDL
PLC18_11.8	P8	November 2018	0.975 ± 0.006	21.17 ± 0.14	21.60 ± 0.33	19.97 ± 0.82	27.79 ± 0.56	15.78 ± 1.02	28.92 ± 2.09	655 ± 29

Sampling points	Dates of comparation	u_{test}	P_{score}	u_{test}	P_{score}	u_{test}	P_{score}	u_{test}	P_{score}	u_{test}	P_{score}	u_{test}	P_{score}	u_{test}	P_{score}	u_{test}	P_{score}
P1	August -	99.40	0.82	99.40	0.82	32.43	2.11	4.74	11.96	3.15	17.01	7.08	10.83	4.85	16.56	16.76	8.74
P2	November	78.53	1.07	78.53	1.07	39.33	2.02	7.16	9.06	6.68	9.15	4.51	15.98	3.65	27.54	19.03	55.45
P8	2018	8.11	0.90	8.11	0.90	2.50	1.80	2.13	4.90	2.43	8.48	0.39	9.10	1.59	10.58	1.24	6.28

* ^{238}U is calculated from the value of ^{235}U and the natural ratio ^{235}U/^{238}U.

behaviour to that of ^{40}K during erosion and accumulation periods could be found. The results showed that total K had lower values in the samples from the erosion period from zone I (PLC18_11.1 and PLC18_11.2); they also show an increase in samples from the same stations during accumulation periods (PLC18_11.8 and PLC18_8.1). In the samples from zone III the results obtained for both samples (PLC18_11.8 and PLC18_8.8) do not present such a strong difference. Moreover, Ca and Ba also displayed a similar change to K, whereas Mg had the opposite behaviour, with higher concentrations during erosion periods and lower concentrations during accumulation periods. Therefore, it could be said that Ca and Ba followed a similar pattern to K. Since it was not possible to analysed Ra through this method and considering that the alkaline earth elements Ra and Ba have similar chemical properties, it was assumed that Ra also followed the pattern of K. Thus, this could also explain why ^{226}Ra and ^{228}Ra have followed a similar distribution to ^{40}K. Thus, these three radionuclides would be transported along with Ca and Ba in the lighter fraction of the sand that moves into and along the beach during erosion and accumulation periods. Therefore, ^{226}Ra and ^{228}Ra could also be used as tracers of the sediment dynamics of the beach.

The results of the SCXRD (Single Crystal X-ray Difraction) allowed the determination that feldspar is anorthoclase ($Ab_{0.73}Or_{0.27}$), clinopyroxene is diopside ($CaMgSi_2O_6$) and olivine is forsterite ($Fo_{0.82}$, Fo = Mg_2SiO_4). The observed cell parameters are reported in Table 5. Both feldspar and clinopyroxene show extended solid solution (i.e. change in composition) that change lattice parameters and thus the angles at which crystal planes diffract. Having an estimation of the chemical composition through SCXRD allowed us to select more appropriate PDF files for matching more precisely the observed d-spacing in the powder X-ray pattern among the large number of available ones. XRPD (Powder X-ray diffraction) results on the studied sand samples were characterised by the presence of abundant feldspar (anorthoclase, $(Na,K)AlSi_3O_8$), calcite (trigonal $CaCO_3$) and aragonite (orthorhombic $CaCO_3$), plus variable amounts of (diopsidic) clinopyroxene and minor amounts of (forsteritic) olivine and amphibole (probably a ferro-hornblende or a ferro-pargasite; cell parameters are $a = 9.872(13)$, $b = 18.100(10)$, $c = 5.304(5)$ Å, $\alpha = 90°$, $\beta = 105.42(11)°$, $\gamma = 90°$, and $V = 914(2)$ Å^3). However, there are modal differences between high energy seasons (erosion periods) and low energy seasons (accumulation periods) in some of the samples as shown on the three diffraction diagrams that appear in Fig. 7.

Fig. 7a shows the comparison of the diffraction diagrams of the samples belonging to station P1 during erosion (PLC18_11.1) and accumulation (PLC8_8.1) periods. There are evidently differences because anorthoclase, calcite and aragonite are reduced in high-energy season, where higher density Mg-rich mineral phases (diopside, amphibole, and minor olivine) have been preferentially concentrated. In low energy seasons, sand predominantly comprises anorthoclase, calcite and aragonite instead. Trace amounts of illite ($K_{1-x}Al_2[Al_{1-x}Si_{3+x}]O_{10}(OH)_2$) were found in both seasons.

In Fig. 7b, the diffraction diagrams of the samples for station P2 are shown. These diagrams display more clearly the difference in mineral content for both seasons in zone I. The feldspar (mainly anorthoclase), calcite and aragonite are absent in high-energy seasons, whereas higher density mineral Fe/Ti oxides (ilmenite, hematite and magnetite) have been concentrated, along with Mg-rich phases (diopside and some olivine). The total rock composition is therefore higher in Mg, whereas Ca remains because of diopside, but its concentration decreases. Potassium, mainly concentrated in feldspar, is highly reduced in high-energy season sediments. In low energy season sediments, anorthoclase (as well as some sanidine $KAlSi_3O_8$ to a lesser degree) and carbonates are

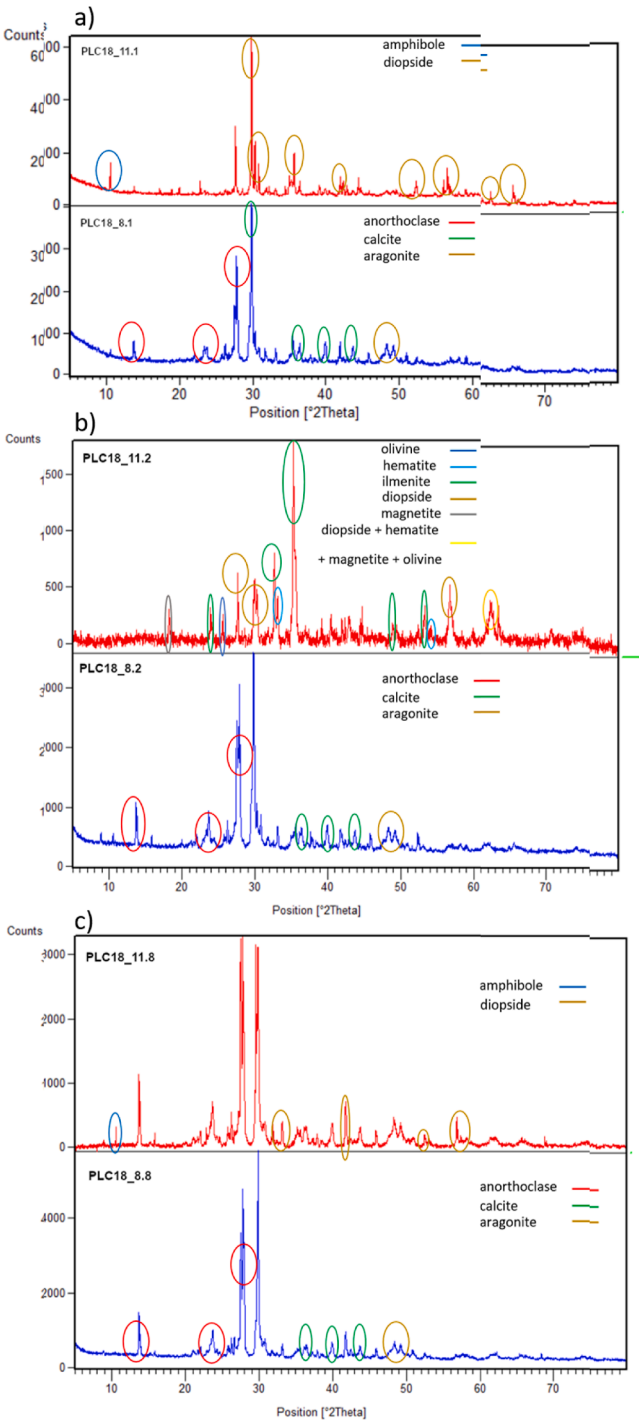

Fig. 7. Comparation of diffraction diagrams in erosion (PLC18_11) and accumulation (PLC18_8) periods for. (a) Samples PLC18_11.1 and PLC18_8.1 (zone I), (b) Samples PLC18_11.2 and PLC18_8.2 (zone I) and (c) Samples PLC18_11.8 and PLC18_8.8 (zone III).

Table 5
Cell parameters and approximate chemical composition of the crystal studied by SCXRD.

	Forsterite $Mg_{0.82}Fe_{0.18}SiO_4$	Diopside $CaMgSi_2O_6$	Anorthoclase $Na_{0.73}K_{0.27}AlSi_3O_8$
s.g.	*Pbnm*	*C2/c*	*C2/m*
a (Å)	4.7689(7)	9.725(3)	8.3036(14)
b (Å)	10.2480(14)	8.8791(11)	12.9749(10)
c (Å)	6.0071(8)	5.2674(7)	7.1522(7)
α (°)	90	90	90
β (°)	90	105.96(2)	116.167(9)
γ (°)	90	90	90
V (Å^3)	293.58(7)	437.31(16)	691.59(15)

s.g. = space group.

predominant, while diopside and amphibole (as well as some phyllosilicate, probably illite) are minor. Olivine has not been observed here but some cristobalite (SiO_2) is present instead.

Finally, Fig. 7c presents the diffraction diagrams of the samples from station P8, belonging to zone III. In this case, feldspar (mainly anorthoclase) calcite and aragonite are the dominant mineral phases in both high and low energy seasons. Sand is only slightly richer in diopside in high energy seasons and some amphibole (and very minor hematite and olivine) also becomes concentrated. This location is protected by an offshore rocky bar and is, therefore, less exposed to tidal changes and to mineral variation because energy in the water is much reduced. Therefore, the selection of minerals as a function of density is not allowed.

The results of the XRPD showed that accumulation periods in zone I, and especially sampling point P2, show that potassium is mainly concentrated in feldspar, probably anorthoclase. These feldspars appear during accumulation periods in zone I and disappear in erosion periods, while being present in zone III all the time. This means that this feldspar, which contains potassium, is present whenever and wherever the activity concentration of ^{40}K is higher. Therefore, it could be said that ^{40}K is tracing the movement of this feldspar contained in the light fraction of the sand along and into the beach, making it a good tracer for beach sediment dynamics. Moreover, the multi-element analysis shows that other elements, like Ba (which is also fractionated in feldspar, usually in trace amounts), follow the same pattern as K. These elements have a similar chemical behaviour to Ra and so it is suggested that ^{226}Ra and ^{228}Ra could also be used as tracers of the beach sediment dynamics.

4. Conclusions

The analysis of the temporal variability of natural radionuclides during this 3 year-long study suggests that the radionuclides ^{226}Ra, ^{228}Ra and ^{40}K in the sand of Las Canteras beach are closely following marine sediment dynamics, together with their parent isotopes. The statistical analysis showed that these three radionuclides present higher activity concentration values in periods with low significant wave height and a NE wave approach direction. These periods are expected in a low energy season when the accumulation of sediments occur on the beach. During high wave height periods the activity concentration of these radionuclides decreased. The ratio $^{226}Ra/^{228}Ra$, previously suggested as a tracer of beach sediment dynamics with a data series of 1 year, did not show any significant differences in erosion or accumulation periods for all of the beach. This indicates that the ratio might not be appropriate to trace sediment dynamics in zones I and II. However, zone III (which is fully protected by the natural offshore rocky bar) showed a ratio value constantly below 1, indicating a constant accumulation period as has been described for this part of the beach. Thus, the lack of significant differences in this area could be pointing out the absence of differences between accumulation and erosion periods. In addition, as already pointed out in the preliminary study, $^{210}Pb_{xc}$ (driven by atmospheric and wind transport) does not seem to be relevant as a tracer of the accumulation/erosion processes of the beach, due to marine sediment transport. Therefore, ^{226}Ra, ^{228}Ra and ^{40}K seem to be more suitable tracers of the beach sediment dynamics during erosion and accumulation periods at Las Canteras beach.

Moreover, the multi-element analysis of total rock composition of the sand that can be found in the different parts of the beach, indicates that Ca and Ba follow a similar dynamic to K. Ba has similar chemical behaviour to Ra and, thus, this could explain the similar pattern to ^{40}K that ^{226}Ra, ^{228}Ra have. This makes them good candidates as tracers of sediment dynamics in coastal areas. In addition, the mineralogical analysis suggests that the activity concentration values found for ^{40}K correspond to the displacement of feldspar grains with high K content, abundant in the light fraction of the sand that moves into and along the beach during accumulation and erosion periods. Thus, ^{40}K seems to be the most fitting tracer of the sediment dynamics at Las Canteras beach.

Declaration of Competing Interest

The authors declare that they have no known competing financial interests or personal relationships that could have appeared to influence the work reported in this paper.

Acknowledgements

The authors of this study acknowledge the help of the Marine Geochemistry division of the Alfred Wegener Institute, Helmholtz Centre for Polar and Marine Research (AWI) in Bremerhaven, Germany for letting them use their facilities for the development of part of this study in the framework of the ERASMUS + traineeship programme.

F.C. acknowledges financial support from the grant "Ricerca Locale 2014", Università di Milano, and by the grant from the Italian Ministry of Education (MIUR) through the 'Dipartimenti di Eccellenza 2018–2022' project.

The authors of this study also acknowledge the financial support by the grant of the Agencia Canaria de Investigación Innovación y Sociedad de la Información Gobierno De Canarias (ACIISI) through the projects CEI2019-10 and CEI2019-13.

Appendix A. Supplementary material

Supplementary data to this article can be found online at https://doi.org/10.1016/j.catena.2021.105705.

References

Alonso, I., 2005. Costa Norte : Playa De Las Canteras, in: Hernández, L., Alonso, I., Mangas, J., Yanes, A. (Eds.), Tendencias Actuales En Geomorfología Litoral. Universidad de Las Palmas de Gran Canaria, La Palmas de Gran Canaria, pp. 219–238.

Alonso, I., 1994. Spatial beach morphodynamics. An example from Canary Islands, Spain. Litoral 94, 169–183.

Alonso, I., 1993. Procesos sedimentarios en la playa de Las Canteras (Gran Canaria). Universidad de Las Palmas de Gran Canaria.

Alonso, I., Pérez Torrado, F.J., 1992. Estudio sedimentológico de la playa de Las Canteras (Gran Canaria). Datos preliminaries. III Congr. geológico España y tomo 2, 131–135.

Alonso, I., Vilas, F., 1996. Variabilidad sedimentaria en la playa de Las Canteras (Gran Canaria). Geogaceta 20, 428–430.

Arnedo, M.A., Rubiano, J.G., Alonso, H., Tejera, A., González, A., González, J., Gil, J.M., Rodríguez, R., Martel, P., Bolivar, J.P., 2017. Mapping natural radioactivity of soils in the eastern Canary Islands. J. Environ. Radioact. 166, 242–258. https://doi.org/10.1016/j.jenvrad.2016.07.010.

Arnedo, M.A., Tejera, A., Rubiano, J.G., Alonso, H., Gil, J.M., Rodriguez, R., Martel, P., 2013. Natural radioactivity measurements of beach sands in gran Canaria, Canary Islands (Spain). Radiat. Prot. Dosim. 156 (1), 75–86. https://doi.org/10.1093/rpd/nct044.

Arriola-Velásquez, A., Tejera, A., Guerra, J.G., Alonso, I., Alonso, H., Arnedo, M.A., Rubiano, J.G., Martel, P., 2019. Spatio-temporal variability of natural radioactivity as tracer of beach sedimentary dynamics. Estuar. Coast. Shelf Sci. 231, 106476. https://doi.org/10.1016/j.ecss.2019.106476.

Balcells, R., Barrera, J.L., Ruiz García, M.T., (Cartographers), 1990. Geological Map 1101-I-II Las Palmas de Gran Canaria, 1:25000 IGME.

Bezuidenhout, Jacques, 2020. The investigation of natural radionuclides as tracers for monitoring sediment processes. J. Appl. Geophys. 181, 104135. https://doi.org/10.1016/j.jappgeo.2020.104135.

Bezuidenhout, J., 2013. Measuring naturally occurring uranium in soil and minerals by analysing the 352keV gamma-ray peak of ^{214}Pb using a NaI(Tl)-detector. Appl. Radiat. Isot. 80, 1–6. https://doi.org/10.1016/j.apradiso.2013.05.008.

Burnett, William C., Bokuniewicz, Henry, Huettel, Markus, Moore, Willard S., Taniguchi, Makoto, 2003. Groundwater and pore water inputs to the coastal zone. Biogeochemistry 66 (1/2), 3–33.

Chabaux, F., Blaes, E., Granet, M., Roupert, R. di C., Stille, P., 2012. Determination of transfer time for sediments in alluvial plains using 238U–234U-230Th disequilibria: the case of the Ganges river system. Comptes Rendus – Geosci. 344, 688–703. https://doi.org/10.1016/j.crte.2012.10.013.

Chabaux, François, Granet, Mathieu, Pelt, Eric, France-Lanord, Christian, Galy, Valier, 2006. ^{238}U–^{234}U-^{230}Th disequilibria and timescale of sedimentary transfers in rivers: clues from the Gangetic plain rivers. J. Geochem. Explor. 88 (1-3), 373–375. https://doi.org/10.1016/j.gexplo.2005.08.078.

Dai, Zhi-Jun, Du, Jin-Zhou, Chu, Ao, Zhang, Xiao-Ling, 2011. Sediment characteristics in the North Branch of the Yangtze Estuary based on radioisotope tracers. Environ. Earth Sci. 62 (8), 1629–1634. https://doi.org/10.1007/s12665-010-0647-7.

Dueñas, C., Gordo, E., Liger, E., Cabello, M., Cañete, S., Pérez, M., de la Torre-Luque, P., 2017. ^{7}Be, ^{210}Pb and ^{40}K depositions over 11 years in Málaga. J. Environ. Radioact. 178–179, 325–334. https://doi.org/10.1016/j.jenvrad.2017.09.010.

Gaspar, L., Webster, R., Navas, A., 2017. Fate of $^{210}Pb_{ex}$ fallout in soil under forest and scrub of the central Spanish Pre-Pyrenees. Eur. J. Soil Sci. 68 (3), 259–269. https://doi.org/10.1111/ejss.2017.68.issue-310.1111/ejss.12427.

Giffin, D., Corbett, D.R., 2003. Evaluation of sediment dynamics in coastal systems via short-lived radioisotopes. J. Mar. Syst. 42 (3-4), 83–96. https://doi.org/10.1016/S0924-7963(03)00068-X.

Guerra, J.G., Rubiano, J.G., Winter, G., Guerra, A.G., Alonso, H., Arnedo, M.A., Tejera, A., Martel, P., Bolivar, J.P., 2017. Computational characterization of HPGe detectors usable for a wide variety of source geometries by using Monte Carlo simulation and a multi-objective evolutionary algorithm. Nucl. Instrum. Methods Phys. Res. Sect. A Accel. Spectrom. Detect. Assoc. Equip. 858, 113–122. https://doi.org/10.1016/j.nima.2017.02.087.

Guerra, J.G., Rubiano, J.G., Winter, G., Guerra, A.G., Alonso, H., Arnedo, M.A., Tejera, A., Gil, J.M., Rodríguez, R., Martel, P., Bolivar, J.P., 2015. A simple methodology for characterization of germanium coaxial detectors by using Monte Carlo simulation and evolutionary algorithms. J. Environ. Radioact. 149, 8–18. https://doi.org/10.1016/j.jenvrad.2015.06.017.

Halliday, Alex N., Lee, Der-Chuen, Christensen, John N., Rehkämper, Mark, Yi, Wen, Luo, Xiaozhong, Hall, Chris M., Ballentine, Chris J., Pettke, Thomas, Stirling, Claudine, 1998. Applications of multiple collector-ICPMS to cosmochemistry, geochemistry, and paleoceanography. Geochemica Cosmochim. Acta 62 (6), 919–940.

Herrera, A., Asensio, M., Martínez, I., Santana, A., Packard, T., Gómez, M., 2018. Microplastic and tar pollution on three Canary Islands beaches: an annual study. Mar. Pollut. Bull. 129, 494–502. https://doi.org/10.1016/j.marpolbul.2017.10.020.

Huang, D., Du, J., Deng, B., Zhang, J., 2013. Distribution patterns of particle-reactive radionuclides in sediments off eastern hainan island, china: Implications for source and transport pathways. Cont. Shelf Res. 57, 10–17. https://doi.org/10.1016/j.csr.2012.04.019.

Hülse, Peter, Bentley, Samuel J., 2012. A ^{210}Pb sediment budget and granulometric record of sediment fluxes in a subarctic deltaic system: the Great Whale River, Canada. Estuar. Coast. Shelf Sci. 109, 41–52. https://doi.org/10.1016/j.ecss.2012.05.019.

IAEA, 2011. ALMERA Proficiency Test : Determination of Natural and Artificial Radionuclides in Soil and Water, Analytical Quality in Nuclear Applications. Vienna.

Karlsson, L., Hernandez, F., Rodríguez, S., López-Pérez, M., Hernandez-Armas, J., Alonso-Pérez, S., Cuevas, E., 2008. Using ^{137}Cs and ^{40}K to identify natural Saharan dust contributions to PM10 concentrations and air quality impairment in the Canary Islands. Atmos. Environ. 42 (30), 7034–7042. https://doi.org/10.1016/j.atmosenv.2008.06.016.

Kipp, L.E., Spall, M.A., Pickart, R.S., Kadko, D.C., Moore, W.S., Dabrowski, J.S., Charette, M.A., 2020. Observational and modeling evidence of seasonal trends in sediment-derived material inputs to the Chukchi Sea. J. Geophys. Res. Ocean. 125, 1–13. https://doi.org/10.1029/2019JC016007.

Li, Wenpeng, Li, Xinxin, Mei, Xi, Zhang, Fan, Xu, Jingping, Liu, Chunru, Wei, Chuanyi, Liu, Qingsong, 2021. A review of current and emerging approaches for Quaternary marine sediment dating. Sci. Total Environ. 780, 146522. https://doi.org/10.1016/j.scitotenv.2021.146522.

Lin, Wuhui, Feng, Yu, Yu, Kefu, Lan, Wenlu, Wang, Yinghui, Mo, Zhenni, Ning, Qiuyun, Feng, Liangliang, He, Xianwen, Huang, Yinlin, 2020. Long-lived radionuclides in marine sediments from the Beibu Gulf, South China Sea: Spatial distribution, controlling factors, and proxy for transport pathway. Mar. Geol. 424, 106157. https://doi.org/10.1016/j.margeo.2020.106157.

López-Pérez, M., Ramos-López, R., Perestelo, N.R., Duarte-Rodriguez, X., Bustos, J.J., Alonso-Pérez, S., Cuevas, E., Hernández-Armas, J., 2013. Arrival of radionuclides released by the Fukushima accident to Tenerife (Canary Islands). J. Environ. Radioact. 116, 180–186. https://doi.org/10.1016/j.jenvrad.2012.09.011.

Mangas, J., Julià-Miralles, M., 2015. Geomorfología y naturaleza de las bajas submareales de Bajo Fernando, Los Roquerillos y La Zabala (NE de Gran Canaria). Geo-Temas 15, 37–40.

Medina, R., Bastón, S., Cánovas, V., Torres, A., Luque, Á., Alonso, I., Sánchez, I., Ortega, A., Rodríguez, S., Martín, J.A., 2006. Estudio integral de la playa de Las Canteras, Technical Report Dirección General de Costas.

Moore, W.S., 2007. Radon and radium isotopes as tracers of coastal mixing and submarine groundwater discharge. Water Environ. News 23, 14–23.

Osvath, I., Tarjan, S., Pitois, A., Groening, M., Osborn, D., 2016. IAEA ' s ALMERA network: supporting the quality of environmental radioactivity measurements. Appl. Radiat. Isot. 109, 90–95. https://doi.org/10.1016/j.apradiso.2015.12.062.

Pittauer, D., Roos, P., Qiao, J., Geibert, W., Elvert, M., Fischer, H.W., 2018. Pacific Proving Grounds radioisotope imprint in the Philippine Sea sediments. J. Environ. Radioact. 186, 131–141. https://doi.org/10.1016/j.jenvrad.2017.06.021.

Pozebon, D., 2002. Marine sediment analysis using inductively coupled plasma optical emission spectrometry. At. Spectrosc. 23, 111–118.

Rigaku Oxford Diffraction, 2020. *CrysAlisPro*, version 1.171.40.71a. Rigaku Corporation, Oxford, UK.

Sanial, V., van Beek, P., Lansard, B., Souhaut, M., Kestenare, E., D'Ovidio, F., Zhou, M., Blain, S., Blain, S., 2015. Use of Ra isotopes to deduce rapid transfer of sediment-derived inputs off Kerguelen. Biogeosciences 12, 1415–1430. https://doi.org/10.5194/bg-12-1415-2015.

Schmincke, H.U., 1993. Geological field guide of Gran Canaria, sixth ed. Pluto-Press, Kiel (Germany).

Schultz, B.B., 1985. Levene' s test for relative variation. Syst. Zool. 34 (4), 449–456.

Shakhashiro, A., Tarjan, S., Ceccatelli, A., Kis-benedek, G., Betti, M., 2012. IAEA-447: a new certified reference material for environmental radioactivity measurements. Appl. Radiat. Isot. 70, 1632–1643. https://doi.org/10.1016/j.apradiso.2012.03.024.

Shapiro, S.S., Wilk, M.B., 1965. An analysis of variance test for normality (complete samples). Biometrika 52, 591–611. https://doi.org/10.2307/2333709.

Sheldrick, G.M., 2015. Crystal structure refinement with SHELXL. Acta Crystallogr. Sect. C Struct. Chem. 71, 3–8. https://doi.org/10.1107/S2053229614024218.

Sun, X., Fan, D., Liao, H., Liu, M., Tian, Y., Zhang, X., Yang, Z., 2020. Variation in sedimentary ^{210}Pb over the last 60 years in the Yangtze River Estuary: new insight to the sedimentary processes. Mar. Geol. 427, 106240. https://doi.org/10.1016/j.margeo.2020.106240.

Tamborski, J., Bejannin, S., Garcia-Orellana, J., Souhaut, M., Charbonnier, C., Anschutz, P., Pujo-pay, M., Conan, P., Crispi, O., Monnin, C., Stieglitz, T., Rodellas, V., Andrisoa, A., Claude, C., van Beek, P., 2018. A comparison between water circulation and terrestrially-driven dissolved silica fluxes to the Mediterranean Sea traced using radium isotopes. Geochim. Cosmochim. Acta 238, 496–515. https://doi.org/10.1016/j.gca.2018.07.022.

Tejera, A., Pérez-Sánchez, L., Guerra, G., Arriola-Velásquez, A.C., Alonso, H., Arnedo, M. A., Rubiano, G., Martel, P., 2019. Natural radioactivity in algae arrivals on the Canary coast and dosimetry assessment. Sci. Total Environ. 658, 122–131. https://doi.org/10.1016/j.scitotenv.2018.12.140.

Thereska, J., 2009. Natural radioactivity of coastal sediments as tracer in dynamic sedimentology. Nukleonika 54, 45–50.

Wakiyama, Y., Onda, Y., Mizugaki, S., Asai, H., Hiramatsu, S., 2010. Soil erosion rates on forested mountain hillslopes estimated using ^{137}Cs and $^{210}Pb_{ex}$. Geoderma 159 (1-2), 39–52. https://doi.org/10.1016/j.geoderma.2010.06.012.

Walder, A.J., Freedman, P.A., 1992. Isotopic ratio measurement using a double focusing magnetic sector mass analyser with an inductively coupled plasma as an ion source. J. Anal. Aromic Spectrom. 7, 571–575.

Wang, Jinlong, Zhang, Weiguo, Baskaran, Mark, Du, Jinzhou, Zhou, Feng, Wu, Hui, 2018. Fingerprinting sediment transport in river-dominated margins using combined mineral magnetic and radionuclide methods. J. Geophys. Res. Ocean. 123 (8), 5360–5374. https://doi.org/10.1029/2018JC014174.

Williams, L.J., Abdi, H., 2010. Tukey 's honestly signiflcant difference test (HSD). Encycl. Res. Des. 2–7.

Yang, Wei-feng, Chen, Min, Zhang, Xin-xing, Guo, Zhi-gang, Li, Guang-xue, Ma, Qiang, Yang, Jun-hong, Huang, Yi-pu, 2013. Thorium isotopes (^{228}Th, ^{230}Th, ^{232}Th) and applications in reconstructing the Yangtze and Yellow River floods. Int. J. Sedim. Res. 28 (4), 588–595. https://doi.org/10.1016/S1001-6279(14)60015-9.

Zheng, Y., Weinman, B., Cronin, T., Fleisher, M.Q., Anderson, R.F., 2003. A rapid procedure for the determination of thorium, uranium, cadmium and molybdenum in small sediment samples by inductively coupled plasma-mass spectrometry: application in Chesapeake Bay. Appl. Geochem. 18, 539–549.